New concepts for nanophotonics and nano-electronics

Nano-manipulation of confined electromagnetic fields with a near-field probe

Benoit Cluzel [a,*], Loïc Lalouat [a], Philippe Velha [b,c,d], Emmanuel Picard [a], David Peyrade [d], Jean-Claude Rodier [c], Thomas Charvolin [b], Philippe Lalanne [c], Emmanuel Hadji [b], Frédérique de Fornel [a]

[a] *Groupe d'optique de champ proche, ICB, UMR CNRS 5209, 9, avenue Alain-Savary, BP 47870, 21078 Dijon cedex, France*
[b] *Laboratoire SiNaPS – MINATEC, Département de recherche fondamentale sur la matière condensée, Commissariat à l'énergie atomique, 17, rue des Martyrs, 38054 Grenoble cedex 9, France*
[c] *Laboratoire Charles-Fabry de l'institut d'optique, Centre national de la recherche scientifique, 91403 Orsay cedex, France*
[d] *Laboratoire des technologies de la microélectronique, Centre national de la recherche scientifique, 38054 Grenoble cedex 9, France*

Available online 12 February 2008

Abstract

While optical near-field microscopy techniques have been devoted to mapping the electromagnetic fields down to the Raleigh limit, an exciting challenge is now to use near-field probes to manipulate in situ the properties of these electromagnetic fields. Here we report the resonance tuning and therefore switching of an ultra-low volume ($V \approx 0.6\ (\lambda/n)^3$) solid state resonator by evanescent interaction with a nanometric dielectric tip. By modelling the tip-nanocavity interaction, we demonstrate that a lossless interaction regime can be achieved in which the tip behaves as a pure optical path length modulator. ***To cite this article: B. Cluzel et al., C. R. Physique 9 (2008).***
© 2007 Académie des sciences. Published by Elsevier Masson SAS. All rights reserved.

Résumé

Nano-manipulation de champs electromagnétiques confinés par une sonde champ proche. Alors que les techniques de microscopie en champ proche optique ont été longtemps dédiées à l'observation des champs électromagnétiques en deçà de la limite de Rayleigh, le défi actuel est d'utiliser les sondes champ proche afin de manipuler in situ champs électromagnétiques. Nous montrons ici qu'il est possible d'accorder et, par suite, de commuter la longueur d'onde de résonance d'un nanorésonateur optique en tirant parti de son interaction évanescente avec une sonde champ proche nanométrique. Nous montrons qu'il est possible d'atteindre un régime d'interaction sans perte dans lequel la sonde se comporte comme un modulateur parfait de trajet optique. ***Pour citer cet article : B. Cluzel et al., C. R. Physique 9 (2008).***
© 2007 Académie des sciences. Published by Elsevier Masson SAS. All rights reserved.

Keywords: Photonic crystal; Nanocavity; Scanning Near-Field Optical Microscopy

Mots-clés : Cristaux photoniques ; Nanocavité ; Microscopie en champ proche optique

---

* Corresponding author.
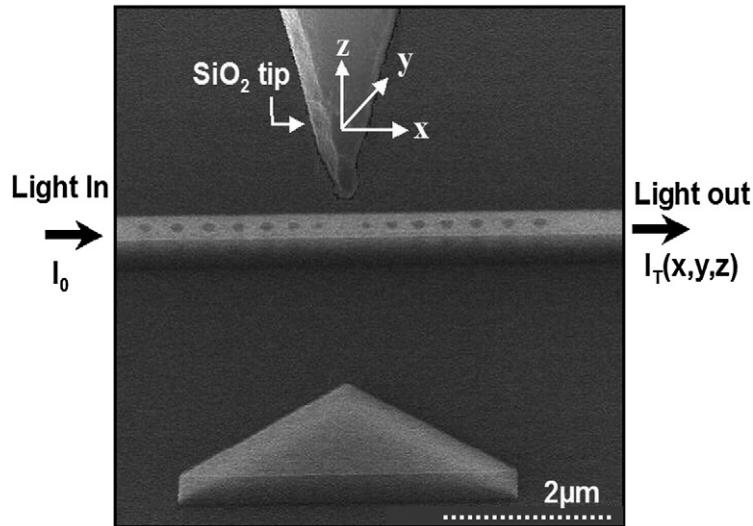 *E-mail address:* benoit.cluzel@u-bourgogne.fr (B. Cluzel).

Fig. 1. Scanning Electron Micrograph views of the nanocavity and the silica tip. The cavity ($N = 3$ in the picture) is formed by the association of two pairs of tapered mirrors etched in a 520-nm wide ridge waveguide. The cavity position is pointed by a triangle on the sample, allowing an optical pre-alignment between the tip and the microcavity. As superimposed, in our experiments, we introduce a silica tip inside the optical near-field of the nanocavity and study the interaction between the tip and the light confined inside the resonator.

Until now, near-field optics has been mostly devoted to the observation of the light distribution inside optical nanodevices using Scanning Near-field Optical Microscopes [1–6] (SNOM). The probe, generally consisting of a dielectric tip, was not supposed to modify the observed system [7]. However, while optoelectronic devices are being miniaturized down to nanometer scale, the interaction between a sub-wavelength tip and a nanocavity is becoming increasingly important [8–10]. In fact, it has been recently predicted numerically [8] that the introduction in the cavity optical near-field of a high optical index tip should permit one to tune the resonance of a solid-state-resonator. The very first attempts to observe such an effect were obtained very recently, but only at the expense of the cavity quality factor (Q) [9,10], which is due to the dramatic losses induced by the presence of the probe [11] near the cavity. If applications such as on-chip information processing, or strong light-matter interaction control by the way of a near-field probe are envisaged, these losses might be a strong limitation. In this article, we propose a system in which a lossless interaction regime between a silica tip and an ultra-low volume high-Q nanocavity is achieved, leading to a strong cavity resonance tuning, without Q-factor and peak-transmittance degradation.

Fig. 1 shows different perspective views, obtained by scanning electron microscopy, of the nanocavity. The nanocavities are composed of two mirrors made of sub-wavelength air holes etched into a SOI ridge waveguide supporting a single transverse-electric (TE) polarized guided-mode. They offer a very small modal volume V of 0.6 $(\lambda/n)^3$ with a single resonance over the 400-nm wide mirror band-gap. While high Q factor were demonstrated [12] for air-standing silicon membrane structures, it is by comparison much more difficult to reach high Q for Photonic Crystals (PC) standing on silicon on insulator (SOI) substrates [13] due to a lower field confinement of the wave guided mode. However, this later configuration, on a substrate, presents a great interest in terms of applications for its greater robustness. So, in order to achieve relative high-Q's, the cavity design carefully takes into account the non-symmetry of the $SiO_2/Si/air$ layer stack. It consists in reducing the radiation losses at the cavity-mirror interfaces by implementing a gradual variation of the transverse mode profiles, i.e. by tapering the defect-ridge guided mode into the associated mirror Bloch mode [14]. Each mirror is formed by a periodic row of N air holes with a 200-nm diameter and a 370-nm periodicity, and by a 4-hole taper with a gradual increase of diameters, from 135 to 200 nm, and of inter-hole distances, from 300 to 350 nm. As the number N of holes in the periodic section of the mirror increases, the mirror modal reflectivity and the cavity Q also increase: as $N \to \infty$, the cavity Q is limited by out-of-plane radiation losses and for $\lambda = 1.6$ µm, the extrapolated value for the unloaded Q is larger than 40 000, the theoretical value being ten times larger [15]. Nanocavities with $N = 2$, 3 and 4 holes have been manufactured using electron-beam lithography followed by a plasma etching in a Silicon-On-Insulator substrate with a 0.38-µm-thick sil-
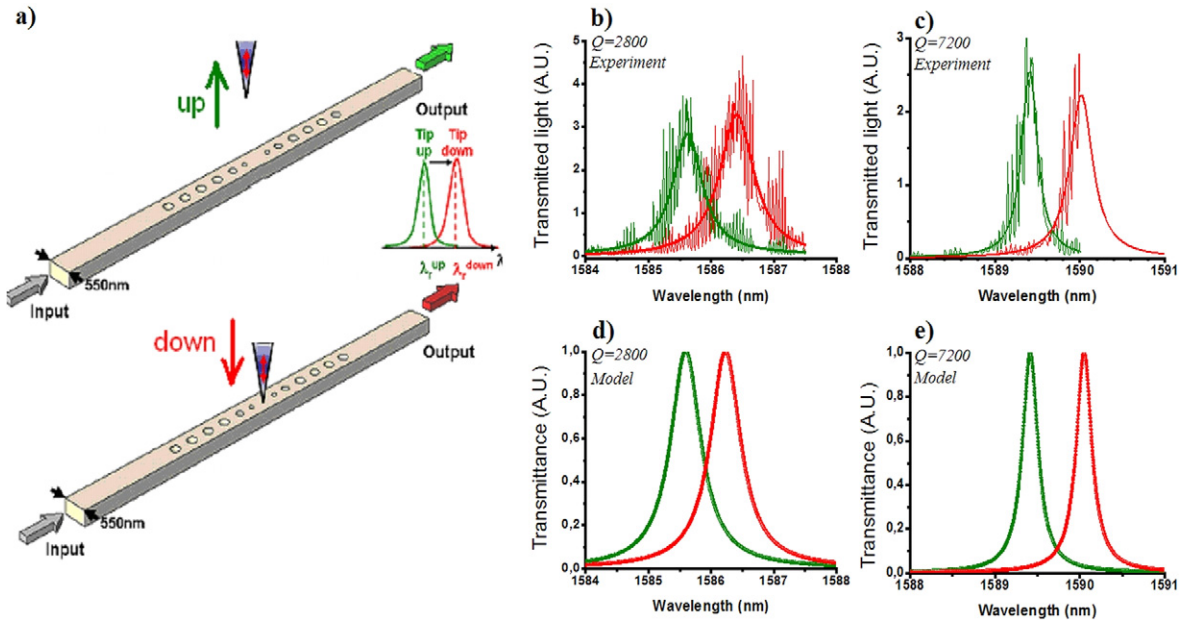
Fig. 2. Cavity tuning by a nanometric tip without Q-factor degradation. (a) Schematic view of the experiment. (b) and (c) Transmission spectra recorded for two tip-cavity distances z, $z^{up} > 100$ nm (green curve) and $z^{down} = 4$ nm (red curve) and for the $Q = 2800$ and $Q = 7200$ cavities. The high-frequency oscillations are due to Fabry–Perot fringes resulting from the bouncing of light between the wafer cleaved facets. Bold curves: Lorentzian fits of the experimental spectra permitting to evaluate the Q-factor with an error bar of 10%. (d) and (e) Fabry–Perot model predictions of the resonance peak red-shift for the two cavities.

icon film and a 2-μm-thick buried oxide layer. Hereafter, only the cavities with $N = 3$ and 4 holes will be considered. Their measured Q's are respectively equal to 2800 and 7200, in agreement with the theoretical values [15].

In the following experiments, we use an end-fire setup to measure the cavity transmission spectra. Light injection from a TE-polarized tuneable laser source and output light collection onto an InGaAs detector are performed by using microscope objectives and monomode polarization-maintaining optical fibres. While accurately keeping these alignments, a ≈250-nm-diameter silica tip mounted on a SNOM is approached above the cavity defect, as shown on Fig. 1. Thanks to a shear-force feedback, the tip is maintained at a fixed distance ($z = 4$ nm) above the wafer. After recording few topographical images of the cavity, the tip is positioned in the centre of the cavity by using piezoelectric scanners. We next recorded the cavity transmission spectra for two different configurations (Fig. 2(a)). For the first configuration (up), the tip is positioned well above the cavity and does not interact with the optical near-field of the cavity mode ($z > 100$). For the second configuration (down), the tip is located just above the cavity ($z = 4$ nm). The recorded spectra exhibit a Lorentzian signature (bold curves in Figs. 2(b) and (c)) with superimposed high-frequency Fabry–Perot fringes resulting from the bouncing of light between the cleaved facets of the wafer. The access ridge waveguides being about 10-mm-long, these oscillations are completely resolved by the 0.01 nm wavelength laser incremental shift used for recording the data.

As shown in Figs. 2(b) and (c), the presence of the tip strongly modifies the resonance of the cavities. It produces a red-shift of the resonance wavelength from $\lambda_r^{up} = 1585.6$ nm to $\lambda_r^{down} = 1586.4$ nm on the $Q = 2800$ cavity. The red-shift value, 0.8 nm, corresponds to a relative shift of $\delta\lambda/\lambda_r = 5.1 \times 10^{-4}$. In the $Q = 7200$ cavity case, this experiment is unfortunately limited by our laser source tuning range that only allows us to observe the ascending side of the red-shifted resonance. However this indicates that the resonance red-shift is up to 0.6 nm. Such values are one order of magnitude higher than those recently obtained by electro-optical modulation of the silicon refractive index [16]. Remarkably and in contrast to the previous works in this field [9,10], the peak-transmittances at resonance and the Q-factor of the cavities are basically unaffected by the presence of the tip near the cavity.

In order to explain these remarkable effects, we have modelled the cavity-tip interaction. Although 3D-vectorial calculations performed for the entire tip-microcavity system allow for an accurate solution of the electromagnetic interaction in the vicinity of the device, they prevent a simple understanding. Indeed the photonic bandgap cavity be-
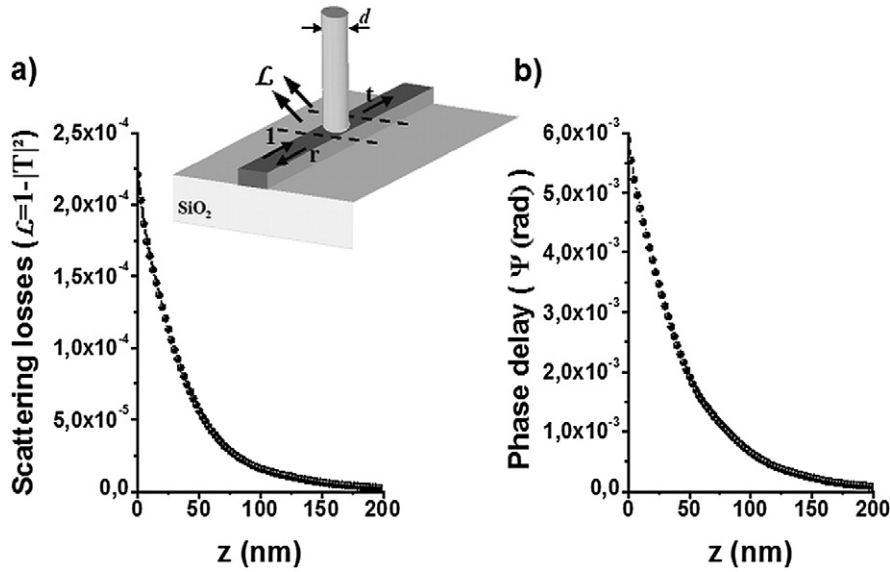
Fig. 3. Scattering by a cylindrical silica tip ($n = 1.5$) as a function of its distance z to a 520-nm-large, 340-nm-high ridge waveguide for a tip having a 300 nm-diameter. (a) Scattering losses ($\mathcal{L}$) and (b) normalized phase delay (Ψ) under the tip approach in the vicinity of the silicon rib waveguide. The inset shows the definition of the tip scattering coefficients, r, t, and $\mathcal{L}$ for the fundamental mode of the ridge waveguide.

haves as a Fabry–Perot resonator in which the fundamental ridge guided mode (effective index $n_{\text{eff}} = 2.7$) is bouncing between the two mirrors. Instead of looking at a global property of the whole device, the basics of the cavity-tip interaction can thus be understood by considering the scattering of the bouncing mode by the tip, namely by considering the modal transmission t and reflection r coefficients of this mode (inset in Fig. 3(a)). Using a fully-vectorial modal method [17], we have calculated these coefficients as a function of the tip-cavity distance (z) for different tip diameters, $d = 200$, 250 and 300 nm, in the range of the actual values used in the experiment. We found that $|r(z)|^2$ is much smaller than $1 - |t(z)|^2$ for any z. Thus, in this weak-backscattering interaction regime, $1 - |t(z)|^2$ also represents out-of-plane radiation losses $\mathcal{L}$ resulting from radiation into the claddings and from scattering into the tip. Figs. 3(a) and (b) show $1 - |t(z)|^2$ and the normalized phase delay $\Psi(z)$, defined by $t(z) = |t(z)| \exp(i\Psi(z))$, as a function of the tip-ridge distance. The most striking result is the smallness of the radiation losses; even for a 300-nm-diameter tip located 4-nm above the ridge, the transmittance $|t|^2$ is larger than 0.9997 (Fig. 3(a)).

Using a Fabry–Perot model and neglecting the tip-reflectance, the transmission T_{cav} of the cavity with a tip located at a distance z above the cavity is readily written as

$$T_{\text{cav}} = \frac{T_M^2 |t(z)|^2}{|1 - r_M^2 t(z) \exp(2ik_0 n_{\text{eff}} D)|} \tag{1}$$

where r_M is the mirror-modal reflectivity coefficient, T_M is the mirror-modal transmittance and D is the defect cavity length. The Fabry–Perot predictions of Eq. (1) have been verified through comparison with a 3D electromagnetic analysis of the whole cavity including the tip. The model shines real insight into the physics of the cavity-tip interaction. In contrast to previous theoretical predictions [8] and rather counter intuitively, but consistently with experimental near-field observations presented hereafter, it predicts that the interaction is independent of the axial location of the tip inside the microcavity; as long as the backscattered light remains smaller than the out-of-plane radiation losses $\mathcal{L}$, $|r|^2 \ll \mathcal{L} \approx 1 - |t|^2$, approaching the tip on a node or an antinode of the cavity mode results in identical effects. It also predicts that, as long as the tip radiation losses are smaller than the cavity losses, $1 - |r_M|^2 < 1 - |t|^2$, i.e. for cavity Q's smaller than 70 000, the tip behaves as a pure path-length modulator which modifies the effective cavity length without sacrificing the cavity Q-factor. Consequently, approaching the tip results only in a red-shift of the resonance wavelength $\Delta\lambda(z)/\lambda = \Psi(z)/[(1 - |r_M|^2)Q]$ as evidenced experimentally and theoretically, see Figs. 2(b)–(e).

Keeping in mind that the weak-backscattering interaction regime discussed earlier is characterized by an interaction nearly independent of the axial location of the tip above the cavity, we investigate the dependence of the relative cavity transmittance ($I_T(x, y)/I_{\text{Max}}$) as a function of the tip scans in the (x, y)-plane at $z = 4$ nm (schematic on
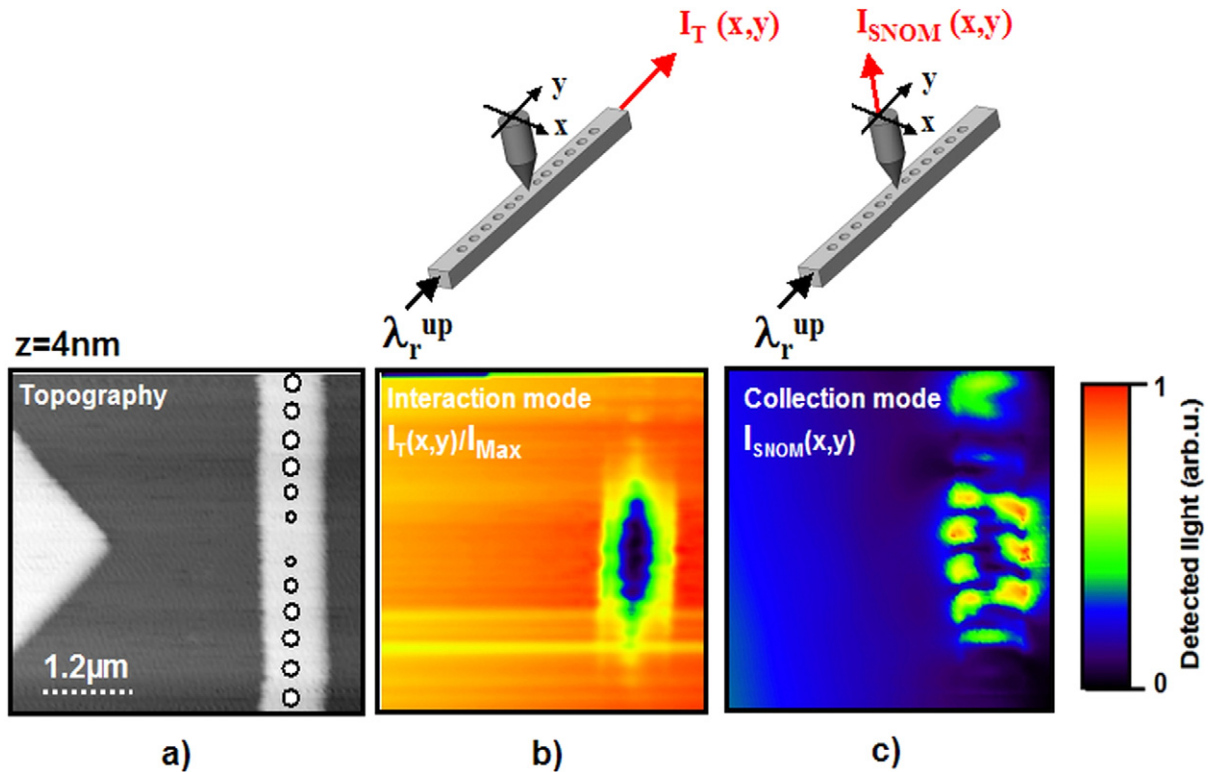
Fig. 4. Experimental near-field pictures recorded in interaction and collection scanning modes. The injected wavelength is set to the resonance wavelength in absence of the tip (λ_r^{up}). (a) Topographical picture corresponding to the tip scan in the (x, y)-plane at $z = 4$ nm. The position of the nanocavity holes is superimposed schematically. (b) Interaction mode picture. The transmittance of the cavity for a $z = 4$ nm tip height as a function of the tip scan in the (x, y)-plane is recorded. The measured transmittance $I_T(x, y)$ is then normalized to the peak-transmittance I_{Max} in absence of the tip. (c) Collection mode picture. The light transmitted through the tip ($I_{SNOM}(x, y)$) is recorded at the same time than $I_T(x, y)$. Colorbar: the brighter the picture, the lower the recorded signal.

Fig. 4(b)). We define such a scanning mode as an interaction scanning mode: as the wavelength is set to the cavity resonance in absence of the tip (λ_r^{up}), the tip-cavity near-field interaction is directly visible by the transmittance decrease associated to the resonance red-shift. The larger the red-shift, the stronger the transmittance decrease. That is what we clearly observe for the two cavities. The experimental interaction map ($I_T(x, y)/I_{Max}$) recorded on the $Q = 7200$ cavity is presented in Fig. 4(b): the cavity transmittance decreases progressively as the tip approaches the cavity center where the light is the strongly confined. This is visible both along the propagation axis (y) and along the transverse direction (x). On each side of the ridge waveguide, the exponential decrease of the transmittance attenuation corresponds to the lateral evanescent decay of the field inside the cavity. In the middle of the cavity where the light is tightly confined, the near-field interaction reaches its maximum, the red-shift value is the widest and thus the transmittance attenuation is the largest.

Remarkably, in contrast to the theoretical predictions of Koenderink et al. [8], and according to our theoretical analysis, the interaction picture ($I_T(x, y)/I_{Max}$), does not reveal any modulations associated to the nodes and antinodes of the cavity mode field. Consequently, approaching the tip from a node or an anti-node of the field inside the cavity leads to an identical effect: the resonance is red-shifted. This represents a clear experimental signature of the weak-backscattering interaction regime discussed earlier and characterized by an interaction nearly independent of the axial location of the tip. As predicted by the Fabry–Perot model, such a counter-intuitive result evidences that the tip behaves as a pure optical path length modulator.

At the same time than the ($I_T(x, y)/I_{Max}$) interaction picture, we also recorded the light transmitted through the tip as a function of the tip position, $I_{SNOM}(x, y)$ (Fig. 4(c)), this scanning mode corresponding to the classical SNOM collection mode used to probe photonic crystal devices. In such a collection mode, because the resonance red-shift is highly dependent of the tip position, the tip cannot collect any light above the cavity as long as the resonance peak
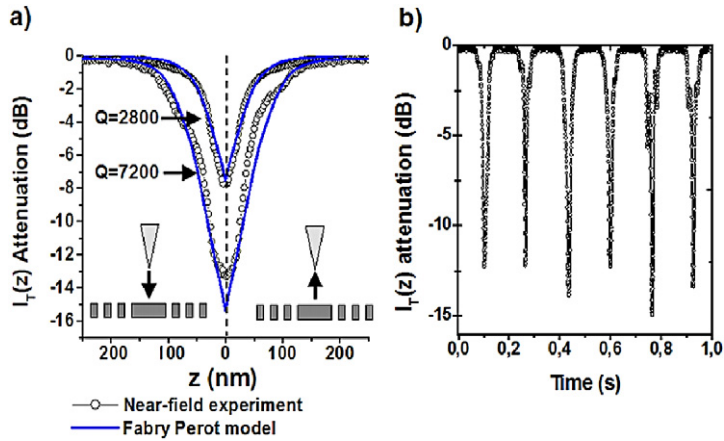
Fig. 5. Switching operation of the cavity-tip nanosystem. (a) Attenuation of the cavity transmittance ($10. \log(I_T(z)/I_{Max})$) as a function of the tip scan along the z-axis. The injected wavelength is set to the resonance wavelength in absence of the tip (λ_r^{up}) and the tip position in the (x, y)-plane is set to the cavity center. As the tip approaches the surface of the cavity ($z < 100$ nm), the transmitted light decreases exponentially. Blue curves (solid lines): model predictions according to Eq. (1). (b) The transmittance attenuation measurement recorded while the tip height is modulated temporally ($z(t)$). (For interpretation of the references to color in this figure legend, the reader is referred to the web version of this article.)

(λ_r^{down}) is red-shifted enough (no overlap with the initial resonance peak (λ_r^{up})). In the present case, as is visible on Fig. 4(c), the tip localized above the middle of the cavity does not collect any light, inducing a large red shift of the resonance. When the tip is moved outside this region, at both sides of the cavity, the interaction between the tip and the cavity is reduced and thus the amount of light penetrating inside the cavity increases and the collected intensity through the tip too. Above the cavity where the light is the most tightly confined, in contrast to all the previous work in this field (references [3] or [4], for example), the tip is now an active element of the investigated system and the picture formed through the tip (Fig. 4(c)) can no more be considered as a field map.

However as it is shown in this article, one can take the benefit of this interaction to built a novel class of near field actuated nanosystems.

For example, the tip-cavity nanosystem can obviously be considered as a nano-switch if we consider the transmittance of the cavity $I_T(z)$ for a given frequency while the tip-cavity distance z is modulated. Fig. 5(a) shows the normalized transmission attenuation for $\lambda = \lambda_r^{up}$, as a function the active parameter z. The tip is positioned above the cavity center in the (x, y)-plane and the z-axis is scanned for tip heights ranging from $z = 4$ to $z = 250$ nm while we record $I_T(z)$ at the same time. The measurements are performed for the two cavities. Two operation regimes may be distinguished. For $z > 100$ nm, the transmitted signal essentially remains constant. For $z < 100$ nm, the signal exponentially drops as the tip approaches the cavity surface. Such an exponential decay is characteristic of a near-field interaction process between the tip and the evanescent field of the cavity mode. Close to contact ($z = 4$ nm), the recorded attenuation reach to -8 and -14 dB of the initial cavity peak transmittance (I_{Max}) for the $Q = 2800$-cavity and the $Q = 7200$-cavity, respectively. As expected, the switching extinction ratio largely depends on the cavity Q-factor which is quantitatively predicted by the Fabry–Perot model as illustrated by the blue (solid lines) curves in Fig. 5(a): from Eq. (1), the switching extinction ratio, defined by $T_{cav}(z = 4 \text{ nm})/T_{cav}(z = 100 \text{ nm})$, is shown to be equal to $[1 + (\Psi_0/\pi F)^2]$, where F is the cavity Finesse and $\Psi_0 = \Psi(z = 4 \text{ nm})$.

At last, the tip height above the cavity is modulated as a function of the time and the transmittance attenuation recorded is plotted on Fig. 5(b). It clearly shows the repeatability of the switching operation. We emphasize here that the time scale limited in our experiment to few Hz could reach the MHz range with the integration of other actuation systems directly nanofabricated on the SOI-chip, the switching time becoming only limited by the mechanical resonance [18]. Even at this early stage of development, the present device may find use in a broad range of applications. Since its tuning range is being compatible with WDM inter-channel wavelength spacing, it can be used for building electromechanical wavelength-division multiplexing routers.

In summary we have shown that a sub-µm dielectric tip, placed in the near field of a high-finesse photonic-bandgap microcavity, behaves as an optical path-length modulator. A 14 dB reversible switching operation together with a 0.8-nm-wide tuning has been observed. Such a system represents a basic building block toward the integration of

on-chip optical switches or tuneable filters. For more fundamental science investigations, the system may also be used for finely matching the cavity-atom resonances in quantum electrodynamics experiments, or for enabling a direct detection and observation of nanoscale motions in NEMS [19]. Finally, we believe that this kind of nanosystems may represent a new step towards a new class of near-field optics active components.

References

 [1] S.I. Bozhevolnyi, et al., Nature 440 (2006) 508.
 [2] W. Dickson, et al., Phys. Rev. B 72 (2005) 094110.
 [3] D. Gérard, et al., Opt. Lett. 27 (2002) 173–175.
 [4] H. Gersen, et al., Phys. Rev. Lett. 94 (2005) 123901–123904.
 [5] B. Cluzel, et al., Appl. Phys. Lett. 85 (2004) 2682.
 [6] F. de Fornel, Evanescent Waves, Springer, Heidelberg, 2001.
 [7] P.M. Adam, L. Salomon, F. de Fornel, J.P. Goudonnet, Phys. Rev. B 48 (1993) 2680.
 [8] A.F. Koenderink, M. Kafesaki, B.C. Buchler, V. Sandoghdar, Phys. Rev. Lett. 95 (2005) 153904.
 [9] I. Märki, M. Salt, H.P. Herzig, Opt. Express 14 (2006) 2969.
[10] W.C.L. Hopman, et al., Opt. Express 14 (19) (2006) 8745.
[11] J.T. Robinson, S.F. Preble, M. Lipson, Opt. Express 14 (22) (2006) 10588.
[12] B. Song, S. Noda, T. Asano, Y. Akahane, Nature Mater. 4 (2005) 207.
[13] Y. Tanaka, T. Asano, R. Hatsuta, S. Noda, Appl. Phys. Lett. 88 (2006) 011112.
[14] C. Sauvan, G. Lecamp, P. Lalanne, J.P. Hugonin, Opt. Express 13 (2005) 245.
[15] P. Vehla, et al., New. J. Phys. 8 (2006) 204.
[16] Q. Xu, B. Schmidt, S. Pradhan, M. Lipson, Nature 435 (2005) 325–327.
[17] E. Silberstein, Ph. Lalanne, J.P. Hugonin, Q. Cao, J. Opt. Soc. Am. A 18 (2001) 2865–2875.
[18] H.G. Craighead, Science 290 (2000) 1532.
[19] M.L. Roukes, Nanoelectromechanical systems face the future, Phys. World 14 (2001) 25–31.